ACS APPLIED BIO MATERIALS

www.acsabm.org Article

Release Rate Studies of 5-Aminosalacylic Acid Coated with Atomic Layer-Deposited Al_2O_3 and ZnO in an Acidic Environment

Jaynlynn Sosa, S. Novia Berriel, Corbin Feit, Taylor M. Currie, Lorianne R. Shultz, Nicholas G. Rudawski, Titel Jurca, and Parag Banerjee*

Cite This: https://doi.org/10.1021/acsabm.2c00750 Read Online

ACCESS | Metrics & More | Article Recommendations | Supporting Information

ABSTRACT: 5-Aminosalicylic acid (5-ASA) is a first-line defense drug used to treat mild cases of inflammatory bowel disease. When administered orally, the active pharmaceutical ingredient is released throughout the gastrointestinal tract relieving chronic inflammation. However, delayed and targeted released systems for 5-ASA to achieve optimal dose volumes in acidic environments remain a challenge. Here, we demonstrate the application of atomic layer deposition (ALD) as a technique to synthesize nanoscale coatings on 5-ASA to control its release in acidic media. ALD Al_2O_3 (38.0 nm) and ZnO (24.7 nm) films were deposited on 1 g batch powders of 5-ASA in a rotatory thermal ALD system. Fourier transform infrared spectroscopy, scanning electron microscopy, and scanning/transmission electron microscopy establish the interfacial chemistry and conformal nature of ALD coating over the 5-ASA particles. While Al_2O_3 forms a sharp interface with 5-ASA, ZnO appears to diffuse inside 5-ASA. The release of 5-ASA is studied in a pH 4 solution via UV−vis spectroscopy. Dynamic stirring, mimicking gut peristalsis, causes mechanical attrition of the Al_2O_3-coated particles, thereby releasing 5-ASA. However, under static conditions lasting 5000 s, the Al_2O_3-coated particles release only 17.5% 5-ASA compared to 100% release with the ZnO coating. Quartz crystal microbalance-based etch studies confirm the stability of Al_2O_3 in pH 4 media, where the ZnO films etch 41× faster than Al_2O_3. Such results are significant in achieving a nanoscale coating-based drug delivery system for 5-ASA with controlled release in acidic environments.

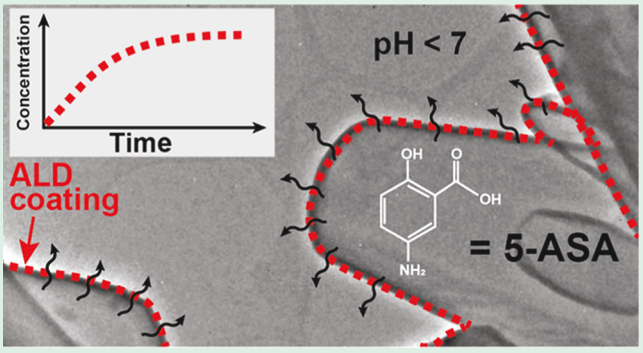

KEYWORDS: *inflammatory bowel disease, 5-aminosalicylic acid, atomic layer deposition, release rate studies, quartz crystal microbalance*

INTRODUCTION

Chronic illnesses affect one out of three people globally.[1] Within this class of diseases, inflammatory bowel disease (IBD) and its two subtypes, ulcerative colitis and Crohn's disease (CD), are classified as chronic illnesses associated with the human gastrointestinal (GI) tract which affects more than 6.8 million people annually.[2] Management and control of these illnesses is done through therapeutic intervention, where the primary goal is to increase patient compliance and reduce medication-based side effects. The primary pharmaceutical molecules to treat IBD are a class of aminosalicylates that have a common moiety: 5-aminosalicylic acid (5-ASA) in their molecular structure.[3] 5-ASA scavenges reactive oxygen species and blocks leukocyte activity and tumor necrosis factor α responsible for chronic inflammation.[4−6]

The key to effective therapeutic intervention is the delivery of 5-ASA at the optimal dose level over sustained periods of time or at a specific location along the GI tract. When 5-ASA is prescribed as an oral formulation, it is commonly absorbed in proximal structures of the small intestine. Therefore, when lesions in distal or even more proximal organs along the GI tract are affected, as it is in the case of CD, it is more difficult to achieve optimal 5-ASA absorption. As a result, delayed release systems and targeted release systems for 5-ASA have been extensively explored.[7,8]

Delayed release systems deliver 5-ASA over long periods of time[9−12] through ethylcellulose coatings corresponding to a treatment time after oral administration of approximately 5 days. These systems include Pentasa and Lialda.[3] However, due to the non-specific slow release of 5-ASA, drug release around severe lesions, especially at colonic sites, is significantly diminished. On the other hand, in targeted release systems, the delivery of 5-ASA takes place mostly at basic to neutral pH, such as that of the colon and rectum. This is achieved through enteric coatings such as Eudragit S that dissolve under basic

Received: August 26, 2022
Accepted: November 30, 2022

pH in the GI tract.[13] These systems include Asacol, Salofalk, and Claversal.[3] Although beneficial to reach distal structures of the GI tract, no systems have been created to release most 5-ASA at more acidic sites in a targeted manner. As a result, the treatment time of these systems is shorter and requires daily medicine intake. Compounding these challenges is the fact that binder and enteric formulations used for coating active pharmaceutical ingredients (APIs) add volume to the pill, limiting API loading efficiencies. This hinders the development of high-dosage oral formulations which are multifunctional, that is, pills that not only release 5-ASA over time but can release at specific locations along the entirety of the GI tract ($1.5 \leq pH \leq 7.5$).

We propose the use of a nanoscale coating technology platform called atomic layer deposition (ALD) to coat 5-ASA powders to address the above challenges. ALD is a gas-phase, conformal, layer-by-layer film growth technique in which control over film thickness and composition can be achieved by sequential and alternative pulsing of gaseous precursor molecules.[14−18] Our rationale to use ALD for coating 5-ASA is based on several factors. First, the use of ALD-based metal oxide chemistries such as Al_2O_3, ZnO, and TiO_2 are well established.[19−21] A key advantage being that ALD occurs at relatively low temperatures (≤150 °C) to maintain the API's viability. Second, the metal oxide candidates presented above are considered biocompatible and present no known toxicity.[22−24] Third, ALD provides non-line-of-sight and self-limiting deposition characteristics that result in highly conformal and pin-hole free films that act as diffusion barriers around particles.[25] Fourth, the use of nanoscale films to coat API powders provides flexibility in terms of adding multi-functionality to pills without adding to its bulk and thus can result in maintaining high dosage levels.

ALD was successfully used on various API powders to (i) change the surface physicochemical characteristics and thereby improve powder flowability and processability[26] or (ii) to achieve controllable release rates of the drug molecule of interest. Specifically, it was shown that by coating irregularly shaped pharmaceutical powders using ALD, the loading efficiency and stability of solid drugs was vastly improved, resulting in better control over delaying drug release times. The molecules previously used as model APIs are acetaminophen, indomethacin, budesonide, and human papilloma virus vaccine powders containing HPV16 L1 capsomeres.[27−31]

In this work, Al_2O_3 and ZnO ALD films are used to coat 5-ASA particles. The motivation for using these two film chemistries is that in acidic environments, Al_2O_3 is relatively stable, while ZnO can be chemically etched. Thus, the use of these two chemistries provides a preliminary proof of concept for coating 5-ASA particles while understanding factors which influence 5-ASA release rates under various conditions encountered in the GI tract, including gut peristalsis (i.e., mechanical attrition) and acidic environment (low pH). Through detailed powder characterization, we establish a basic understanding of the interaction chemistry of the ALD film with the underlying 5-ASA. Studies of ALD Al_2O_3-coated 5-ASA under various stirring conditions mimicking gut peristalsis are conducted to highlight the importance of particle attrition on release rates. A comparison of release rates of ALD Al_2O_3- and ALD ZnO-coated 5-ASA under acidic (pH = 4) conditions is studied and quantified to highlight the importance of chemical interaction of the coatings with the gut microenvironment.

EXPERIMENTAL DETAILS

Synthesis of the ALD-Coated 5-ASA Powder. 5-ASA powders (CAS 89-57-6, 95% purity) with a molecular weight of 153.14 g/mol were purchased from Sigma-Aldrich. The powder was batched into 1 g quantity of material for coating using ALD. A home-built viscous flow, rotatory thermal ALD reactor was used to coat 5-ASA powder via ALD and has been described in detail elsewhere.[25] Briefly, the ALD reactor consisted of a horizontal tube furnace (single zone Lindberg Blue M) with a 7.62 cm core diameter and a length of 61 cm. The upstream side of this furnace was connected to a gas manifold with precursors attached via VCR fittings to ALD Swagelok valves. The valves were controlled via process recipes written with a LabVIEW control software. A digital mass flow controller (Parker Porter Series II 601CV) was used to control the flow of argon (Airgas, 99.999%) during the purge steps. A Leybold Trivac vacuum pump (with Fomblin oil) was used to pump the furnace reactor to a base pressure of ∼13.33 Pa. Pressure was monitored via an MKS 910 DualTrans Transducer.

A rotatory barrel reactor was used to load 5-ASA powders inside the furnace ALD system. This system has been described in detail elsewhere.[25] Briefly, the rotatory barrel reactor was made from stainless steel and measured 5.08 cm in length, 3.81 cm in outer diameter, and 2.79 cm in inner diameter. To avoid powders from agglomerating with each other or sticking to the inner walls of the reactor, a PTFE tube from McMaster-Carr was cut to fit the inside dimensions of the reactor. The powder sample was enclosed inside the barrel with a stainless steel cap machined with four screw slots. In addition, the cap had openings for gases to flow in, through, and out of the barrel reactor. The entire assembly was loaded into the furnace reactor from the load lock. A magnetically coupled arm (from Transfer Engineering and Manufacturing) was used to slide the rotatory reactor inside the furnace. An external stepper motor was then used to rotate the rotatory reactor along its longitudinal axis inside the furnace through a magnetically coupled gear assembly at 8 rpm. The constant tumbling action ensured that the powder was in constant motion during the ALD process, thus exposing the entire batch of powder to the ALD precursors.[32]

All ALD processes were conducted at 120 °C. For Al_2O_3 coating, trimethyl aluminum (TMA, CAS 75-24-1, ≥97% purity, Sigma-Aldrich) and deionized (DI) water (Direct-Q Millipore) were used. For ZnO, diethyl zinc (DEZ, CAS 557-20-0, ≥52 wt %, Sigma-Aldrich) and DI water were used. The recipe for Al_2O_3 (ZnO) consisted of 1 s pulse of TMA (DEZ) and 0.5 s pulse of DI water. In between each pulse, the ALD furnace was purged with a 20 s flow of argon at 75 standard cubic centimeter per minute (sccm). This constituted one cycle of the ALD process. These steps were repeated until a specific number of cycles were met. After the process was completed, the rotatory barrel reactor was unloaded, and the powder was collected and measured. The yield of the powder collected was ≥90% (≥0.9 g) after each run, indicating a minimal powder loss during the ALD process. Two standard recipes were run. One batch of 5-ASA was subjected to 300 cycles of Al_2O_3 ALD (300CyAl_2O_3@5-ASA); this corresponded to a thickness of 33.0 nm on a planar silicon substrate. Another batch of 5-ASA was subjected to 200 cycles of ZnO ALD (200CyZnO@5-ASA); this corresponded to a thickness of 30.6 nm on a planar silicon substrate. Details on the procedure for thickness measurement are provided below.

To measure ALD film thickness, separate coupons of silicon were run, with the exact processes, in a stationary reactor and measured ex situ using a J.A. Woollam M2000 spectroscopic ellipsometer with a wavelength range from 280 to 1690 nm. All optical models for thin-film analysis were built in J.A. Woollam's Complete Ease software.

Powder Characterization. Fourier transform infrared (FTIR) microscopy was performed on a Shimadzu AIM-9000 FTIR microscope. Attenuated total reflectance (ATR, Ge prism) FTIR was performed for each sample where the spectra were obtained by measuring a 100 × 100 μm spot size by 400 scans in the range from 700 to 4000 cm^{-1}, with a resolution of 4 cm^{-1}. The powders were placed on a 5 × 5 mm Si wafer (Ted Pella, Inc.) for measurements,

https://doi.org/10.1021/acsabm.2c00750
ACS Appl. Bio Mater. XXXX, XXX, XXX−XXX

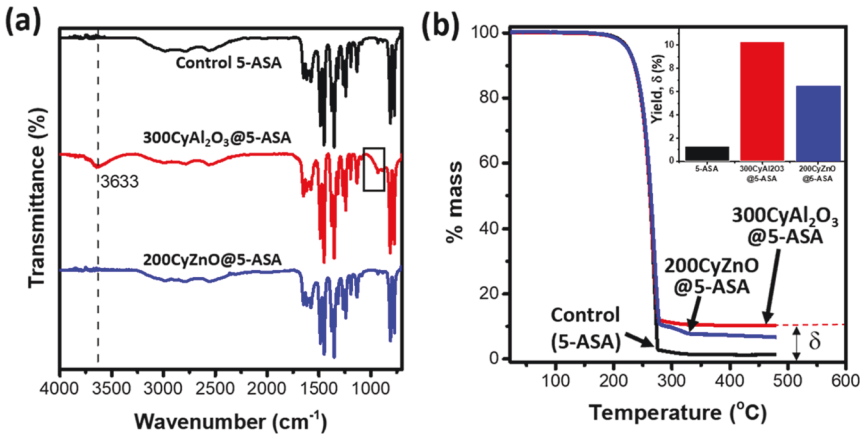

Figure 1. (a) ATR-FTIR spectrum of control 5-ASA, 300CyAl$_2$O$_3$@5-ASA, and 200CyZnO@5-ASA powders. For the Al$_2$O$_3$-coated powder, the broad peak at 3633 cm^{-1} is identified as OH-stretching, while the boxed region (850−1050 cm^{-1}) shows the Al−O bonding. (b) TGA data of control (uncoated), 300CyAl$_2$O$_3$@5-ASA, and 200CyZnO@5-ASA. The final ceramic yield is labeled "δ". The inset shows a histogram plot of δ.

and a section of wafer without any powder was measured as the background. All spectra were baseline-corrected, with CO_2 correction performed as necessary, within the AIMsolution analysis software. Thermogravimetric analysis (TGA) of the powders was conducted on an ISI TGA-1000 instrument, housed inside an inert nitrogen atmosphere glovebox, using Pt sample pans and a 5 cm^3/min flow of UHP N_2. The uncertainty in the mass measurement of the instrument is ±0.05 μg. The following protocol was conducted for all TGA experiments: 20−100 °C at a ramp rate of 20 °C/min, followed by 100−500 °C at a ramp rate of 5 °C/min. The following mass of each sample was used: 2.14 mg of 5-ASA, 2.16 mg of 300CyAl$_2$O$_3$@5-ASA, and 2.17 mg of 200CyZnO@5-ASA.

To characterize the morphology of 5-ASA powder before and after Al$_2$O$_3$ and ZnO ALD, a Hitachi benchtop scanning electron microscope (SEM) with a 15 keV electron beam was used. A small amount of powder was placed on the SEM holder using double-sided carbon tape. The powder was observed at an indicated magnification of 1200× using a fast scan mode. Energy-dispersive spectroscopy (EDS) was conducted using a Bruker Quantax EDX detector. The associated software from Bruker was used for elemental identification of the 5-ASA powders, 300CyAl$_2$O$_3$@5-ASA, and 200CyZnO@5-ASA. The X-ray counts were maximized by scanning large volumes of 5-ASA at multiple spots. At least three different regions on the samples were observed and measured.

Scanning/transmission electron microscopy was performed on the 300CyAl$_2$O$_3$@5-ASA particles using an FEI Tecnai F30 S/TEM operated at 120 keV and equipped with a bottom-mounted Gatan Multiscan 794 digital camera, a Fischione Instruments model 3000 high-angle annular dark-field (HAADF) STEM detector, and an EDAX r-TEM superultrathin window Si(Li) EDS system; both bright-field TEM (BF-TEM) and HAADF-STEM imaging were performed along with STEM-EDS mapping of Al, O, and C. TEM samples of 300CyAl$_2$O$_3$@5-ASA were prepared by making a 50:50 = H_2O/isopropyl alcohol (IPA) solution in a 1 mL centrifuge tube and adding a small amount of 300CyAl$_2$O$_3$@5-ASA particles. The mixed solution (10 μL) was then dropped onto a 300 mesh Cu grid (63 μm grid openings) with a lacey C support film (SPI Supplies Inc.) and allowed to dry overnight.

Similarly, scanning/transmission electron microscopy was also performed on the 200CyZnO@5-ASA particles but using an FEI Themis Z S/TEM with the Cs probe correction operated at 200 kV and equipped with a bottom-mounted FEI Ceta 16M CMOS camera, a Fischione Instruments model 3000 high-angle annular dark-field HAADF-STEM detector, and a SuperX windowless Si drift detector EDS system (solid angle of collection = 0.67 sr). Both high-resolution TEM (HR-TEM) and HAADF-STEM imaging were performed along with STEM-EDS mapping of Zn, O, and C. For HR-TEM imaging, the beam current was set to 300 pA, and a 60 μm objective aperture was used (resulting in ∼15 mrad semiangle of collection). For HAADF-STEM imaging and STEM-EDS mapping, the probe semiangle of convergence was 9 mrad with a probe current of ∼60 pA. It should be noted that the 5-ASA particles were susceptible to beam-induced damage during S/TEM analysis at 200 kV, often experiencing severe warping upon accumulation of a sufficiently high electron dose. Thus, the currents used for S/TEM analysis at 200 kV (as well as the analysis time used for STEM-EDS mapping) were selected to limit the effects of beam-induced damage, so the obtained data was accurately representative of the 200CyZnO@5-ASA particles. Unlike the TEM samples of 300CyAl$_2$O$_3$@5-ASA particles, the TEM samples of 200CyZnO@5-ASA particles were prepared using an entirely dry method; a small amount of 200CyZnO@5-ASA powder was directly placed onto a 300-mesh Cu grid (63 μm grid openings) with a lacey C support film (Ted Pella, no. 01895). The grid was then picked up using a pair of locking tweezers and shook very gently to disperse the particles over the grid; dry air was subsequently used to remove any macroscopically visual particle clusters from the grid. At least two different particles per sample were observed and measurements were taken.

Quartz crystal microbalance studies of the etch rates of ALD Al$_2$O$_3$ and ZnO films were carried out using an SRS QCM200 system. The AT-cut quartz crystals with patterned Cr−Au electrodes and a resonance frequency of 5 MHz (from SRS) were used. The quartz crystals were 2.54 cm in diameter and were coated with 300 cycles and 200 cycles of Al$_2$O$_3$ and ZnO ALD, respectively, using the same precursors as described previously. We note that ALD on QCMs was performed using a Fiji Gen2 ALD commercial system from Veeco. It is not expected that the film composition or properties is hardware dependent.

After ALD, the QCM probe was loaded with a coated crystal, and the frequency and resistivity were zeroed prior to each run. The QCM was submerged into an 80 mL beaker with 80 mL of DI water and a stirring rod rotating at 150 rpm. After 3 min of collecting the baseline, 0.678 μL of HCl was pipetted into the solution to achieve a pH 4 acidic solution. The mass loss (μg/cm^2) over time was extracted in real time until no significant mass loss could be measured on the QCM, thus indicating that the films were fully etched from the surface of the crystal.

Release Rate Studies. UV−vis spectroscopy was used as the method of choice for identifying 5-ASA in low-pH solutions. To conduct static tests, a Shimadzu ultraviolet−visible (UV−vis) 1800 scanning spectrophotometer was used to identify 5-ASA's signature peak[33] at 298 nm. Quartz cuvettes (10 mL) with a 1 cm path length were filled with hydrochloric acid (HCl, ACS reagent 37% (w/w) from MilliporeSigma) solution maintained at pH 4. After the UV−vis spectrophotometer was auto-zeroed and baselined, known amounts of

https://doi.org/10.1021/acsabm.2c00750
ACS Appl. Bio Mater. XXXX, XXX, XXX−XXX

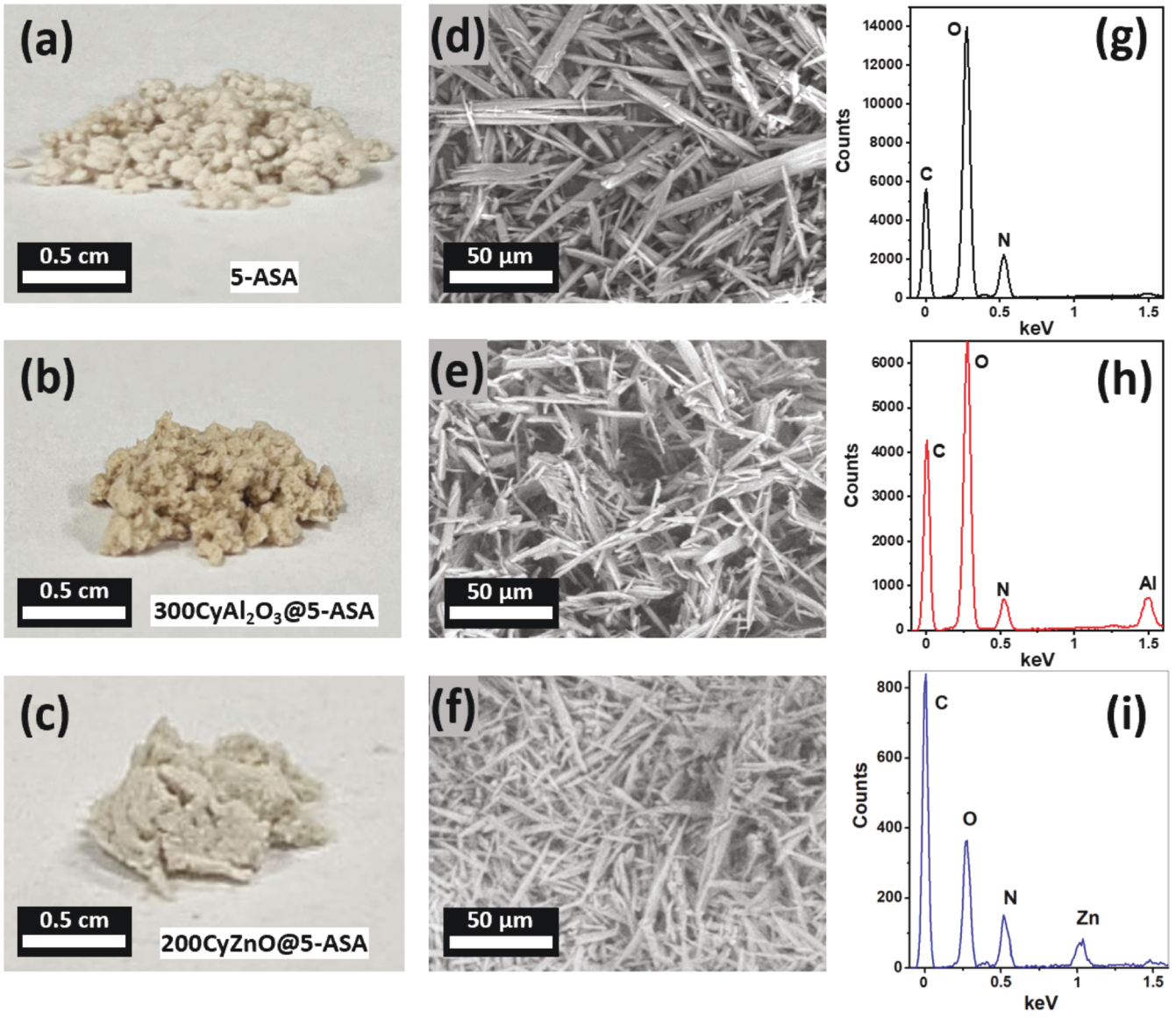

Figure 2. Optical images of (a) control 5-ASA, (b) 300CyAl$_2$O$_3$@5-ASA, and (c) 200CyZnO@5-ASA. SEM images of (d) control 5-ASA, (e) 300CyAl$_2$O$_3$@5-ASA, and (f) 200CyZnO@5-ASA. EDS spectrum of (g) control 5-ASA, (h) 300CyAl$_2$O$_3$@5-ASA, and (i) 200CyZnO@5-ASA.

5-ASA powder (70 μg/mL) were dropped into the sample cuvette and scanned over a wavelength range from 190 to 1100 nm.

All release rate studies of 5-ASA were performed in triplicate using 8 mg powder batches. An Agilent Technologies Cary 60 UV−Vis spectrophotometer, equipped with a 1 cm path length fiber optic probe (C Technologies Inc.), was used to monitor the 298 nm peak. The probe was inserted into 100 mL of HCl solutions maintained at pH 4. This acidic medium was made by adding 0.848 μL of HCl to a 100 mL graduated cylinder and brought up to volume with DI water. The HCl solutions were placed on a magnetic stirring plate, and the solution was stirred at various rotations per minute (rpm). For the experiments reported, three fixed rpm were used: 400, 23, and no stir (i.e., 0 rpm). Since the peak of interest for 5-ASA was found to be at 298 nm, the UV−vis spectrophotometer was set to collect 999 scans from a range of 200−400 nm, every 5 s.

RESULTS AND DISCUSSION

To establish the viability of 5-ASA after ALD, we study the FTIR spectra of the samples first. The detailed FTIR spectrum of uncoated 5-ASA is well studied in the literature[34−37] and is also provided in Supporting Information S1 for the present powder along with the peak assignments table. We provide a comparison between the ATR-FTIR spectra of the control (i.e., uncoated 5-ASA), 300CyAl$_2$O$_3$@5-ASA, and 200CyZnO@5-ASA in Figure 1a. All ATR-FTIR spectra, which measures the bulk powder, contain characteristic 5-ASA peaks, including those at 1354 (C−N stretching), 1452 and 1487 (aromatic C−C stretching), 1620 (N−H bending), 1649 (C═O stretching), and a broad band from 2200 to 3200 cm^{-1} (hydrogen bond vibrations).[34] The broad peak centered at 3633 cm^{-1} in the 300 cycle ALD Al_2O_3 spectrum is due to O−H stretching and the broad peak from 850 to 1050 cm^{-1} is attributed[19] to amorphous Al_2O_3. Zn−O bands occur at wavenumbers below 700 cm^{-1} and thus are not seen in our spectra.[38−40] As a further confirmation for the thermal stability of the 5-ASA powder, we provide in Supporting Information S2 the ATR-FTIR spectra of the control and 5-ASA powder baked at 200 °C under vacuum (16 Pa). All peaks remain intact. This suggests that the 5-ASA powder is chemically stable to a temperature of at least 200 °C for 8 h under vacuum.

https://doi.org/10.1021/acsabm.2c00750
ACS Appl. Bio Mater. XXXX, XXX, XXX−XXX

TGA was conducted in an inert N_2 atmosphere, and the results are shown in Figure 1b. The melting point for 5-ASA is given as 283 °C (from specification sheet, Sigma-Aldrich), while others[41] have reported a melting point of 278 °C and a degradation temperature of 298 °C. Thus, any change to the mass loss behavior would indicate degraded physical and chemical characteristics of 5-ASA. All the three TGA curves resulted in approximately the same shape, with mass loss beginning at ∼200 °C and ending at ∼280 °C. The ceramic yield "δ" of the control, 5-ASA, was 1.32%. The 300CyAl$_2$O$_3$@5-ASA on 5-ASA ended with δ = 10.30%, and the 200CyZnO@5-ASA had δ = 6.50%. The inset in Figure 1b highlights these changes to δ. The greater ceramic yield of the ALD-coated 5-ASA powders is consistent with a thicker Al_2O_3 film on 5-ASA compared to the ZnO-coated sample (discussed below). TGA data along with the first derivative of individual samples are shown in Supporting Information S3. The first derivative of the TGA curves resulted in inflection points at 271.8 °C for 5-ASA, 267.9 °C for 300CyAl$_2$O$_3$@5-ASA, and 269.6 °C for 200CyZnO@5-ASA, showing a minimal change in the powder characteristics upon ALD.

To ascertain the physical morphology of the 5-ASA particles, optical images were taken for control, 300CyAl$_2$O$_3$@5-ASA, and 200CyZnO@5-ASA. These are shown in Figure 2a−c, respectively. The as-received 5-ASA is light beige in color, whereas the 300CyAl$_2$O$_3$@5-ASA powder is darker. There is no change in color observed for 200CyZnO@5-ASA.

Figure 2d shows the morphology of the 5-ASA powder at a magnification of 1200×. 5-ASA has a "needle"-like crystalline structure,[42,43] and a high degree of aggregation among the 5-ASA particles is observed. This behavior is likely due to intramolecular and van der Waals interactions between the particles and the hydroscopic nature of 5-ASA.[32] The morphology of the particles remains intact through deposition of both 300 cycle Al_2O_3 ALD (Figure 2e) and 200 cycle ZnO ALD (Figure 2f).

Figure 2g shows the EDS spectrum of control 5-ASA. High counts of carbon (0.277 keV), oxygen (0.392 keV), and nitrogen (0.525 keV)[44] are observed, consistent with the elements present in the 5-ASA molecule. 300CyAl$_2$O$_3$@5-ASA shows an additional Al peak at 1.486 keV (Figure 2h) and suggests that the powders have been coated with Al_2O_3 ALD. Similarly, 200CyZnO@5-ASA (Figure 2i) shows an energy peak corresponding to the presence of Zn (1.012 keV). Once again, the emission of X-rays corresponding to X-ray energies for Zn suggests the presence of a ZnO ALD coating on 5-ASA.

300CyAl$_2$O$_3$@5-ASA was analyzed under BF-TEM. A typical cluster of 5-ASA particles is shown in Figure 3a. Notice that the needle-like morphology observed previously in SEM images is visualized as a large conical structure at higher magnification under the TEM. The ALD film can be observed as a dark conformal outline to the particles. This is typical of the ALD coating behavior on particles and highlights the non-line-of-sight deposition characteristic of ALD.[25] To analyze the film thickness, Figure 3b was captured at a higher magnification. At this magnification, the Al_2O_3 film thickness was measured using ImageJ software, and the resulting thickness was found to be 38 ± 2.1 nm around the perimeter of the coated 5-ASA particle. For a 300 cycle ALD process, this corresponds to a growth per cycle of 0.126 nm/cycle. The growth per cycle agrees with the typical growth per cycle for Al_2O_3 ALD, which is 0.11−0.13 nm/cycle.[45]

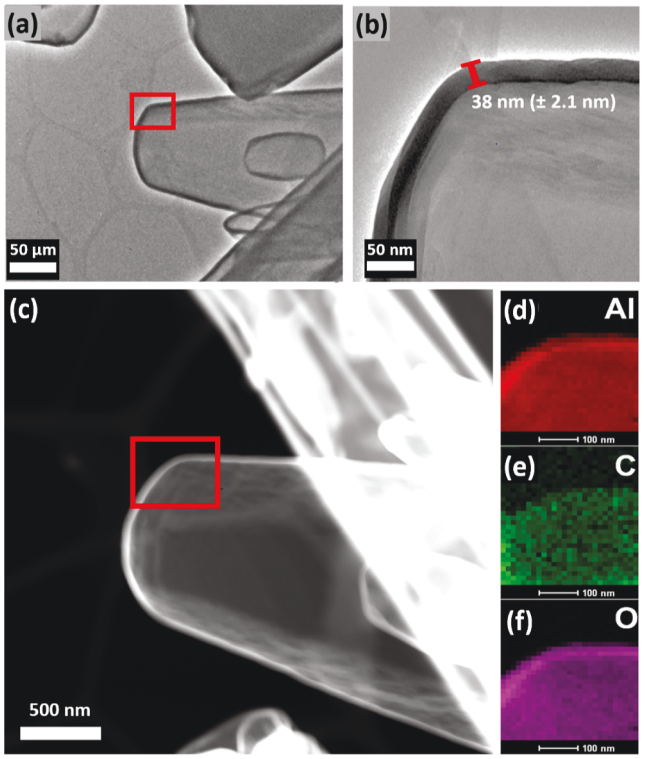

Figure 3. (a) Low-magnification BF-TEM image of 300CyAl$_2$O$_3$@5-ASA. (b) High-magnification BF-TEM image from the red box in (a) showing the conformal nature of the Al_2O_3 ALD film with a shell thickness of 38.0 ± 1.2 nm. (c) HAADF-STEM image of 300CyAl$_2$O$_3$@5-ASA particle. The red box shows the region mapped for EDS analysis. STEM-EDS mapping of 300CyAl$_2$O$_3$@5-ASA showing (d) Al, (e) C, and (f) O.

The 300CyAl$_2$O$_3$@5-ASA particle was also imaged in the dark-field mode (Figure 3c) to highlight the presence of the Al_2O_3 layer. STEM-EDS mapping was performed, and in Figure 3d, the Al elemental map is shown with higher intensity for Al at the perimeter of the 5-ASA particle. This signifies the presence of elemental Al on the surface of the particle as a coating.[46,47] Figure 3e shows the carbon signal with a background from the lacey carbon of the TEM copper grid. The primary carbon still appears to originate from 5-ASA. Figure 3f shows the oxygen distribution with a higher concentration at the edge, signifying that, similar to Al, the O presence is stronger on the surface, that is, from the Al_2O_3 ALD film.

Figure 4a shows the HR-TEM image of the 200CyZnO@5-ASA particle. As in the case of 300CyAl$_2$O$_3$@5-ASA, the ZnO film is also observed as a conformal layer around 5-ASA. The thickness of the film is measured to be 24.7 ± 2.8 nm. For a 200 cycle process, this corresponds to a growth per cycle of 0.12 nm/cycle and is lower than the usually reported growth per cycle of 0.17 nm/cycle.[48] We note that the film is polycrystalline in nature. This is to be expected as ALD ZnO, compared to ALD Al_2O_3, is deposited in its crystalline state even at low (≥100 °C) deposition temperatures.[49] Finally, we observe infiltration of ZnO inside the 5-ASA particle. The infiltration extends tens of nanometers inside the 5-ASA surface. This result is different from the Al_2O_3-coated sample, which forms a clear, sharp interface with 5-ASA. HAADF-STEM imaging was also performed to further highlight the presence of the ZnO film, as shown in Figure 4b. The ZnO

https://doi.org/10.1021/acsabm.2c00750
ACS Appl. Bio Mater. XXXX, XXX, XXX−XXX

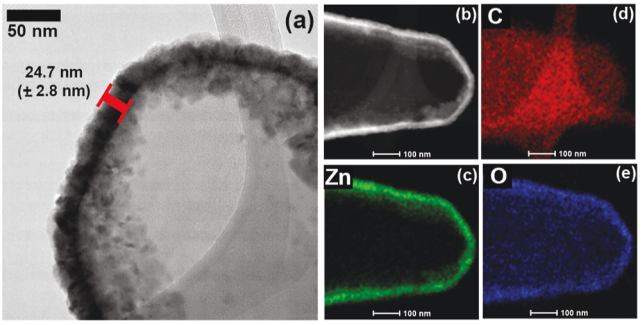

Figure 4. (a) HR-TEM image of 200CyZnO@5-ASA showing a ZnO shell thickness of 24.7 ± 2.8 nm. (b) HAADF-STEM of the 200CyZnO@5-ASA particle. STEM-EDS maps of (c) Zn, (d) C, and (e) O.

crystals can be seen inside 5-ASA in the contrast image as well. STEM-EDS mapping of Zn, C, and O in the same area is shown in Figure 4c–e, respectively. The Zn elemental map supports the observation that ZnO penetrates the 5-ASA particle. We hypothesize that the lower growth per cycle and the diffusion of ZnO inside 5-ASA are correlated. The initial pulses of DEZ could infiltrate the 5-ASA surface and cause growth of subsurface ZnO. As a result, the final thickness obtained could be lower. This is not unreasonable as the largest interplanar spacing[35] for crystalline 5-ASA is 0.59 nm, and DEZ can be approximated as a 0.52 nm-long one-dimensional molecule.[50] Taken together, the TEM results from 300CyAl_2O_3@5-ASA and 200CyZnO@5-ASA powders indicate that the ALD process deposits conformal films around the 5-ASA particles. The thickness measurements are in line with TGA results (Figure 1b), which show a ceramic yield (δ) that is higher for 300CyAl_2O_3@5-ASA (38.0 nm) compared to 200CyZnO@5-ASA (24.7 nm).

To understand the etching rate of Al_2O_3 and ZnO ALD films, QCM crystals were coated by ALD. The inset on the lower right of Figure 5a shows a QCM crystal and its diameter corresponding to 1 inch (25.4 mm) and a gold electrode surface area of 1.267 cm^2. The crystal was coated with 300 cycle Al_2O_3 corresponding to a final thickness of 33 nm measured via ellipsometry on planar Si. After film deposition, the crystal was loaded onto a QCM holder and was placed in 80 mL of DI water maintained at room temperature and with a rapidly rotating stir bar at the bottom of the beaker. The initial mass per square centimeter on the QCM crystal was around 14 $\mu g/cm^2$. After achieving a steady state in the resonance frequency (i.e., ~5 MHz) of the crystal (for approximately 4 min), 0.625 μL of HCl was pipetted into DI water to turn the solution acidic (corresponding to pH 4; 0.0001 M HCl). The low pH did not etch the Al_2O_3 coating due to this material's resistance to acidic media.[17] The slope of the curve corresponds to the etch rate of the film, and a slope of 0.000169 $\mu g/cm^2/s$ was extracted. In other words, 0.000169 μg of Al_2O_3 was etched away per cubic centimeter of the coated crystal per second. Given that the density[51] of amorphous ALD Al_2O_3 is 3.1 g/cm^3, the above etch rate corresponds to 0.0005 nm/s. This etch rate can be compared to those reported[52,53] for untreated ALD Al_2O_3, where, for example, under acidic conditions (1 M H_2SO_4), 40 nm films can be removed in 2 days, yielding an etch rate of 0.0002 nm/s. However, for the purpose of our experiments and with the timelines involved for 5-ASA release, these etch rates can be considered to be low.

In contrast, a different QCM crystal was coated with 200 cycle ZnO ALD. The thickness measured via ellipsometry was 27 nm on planar Si. The starting mass per square centimeter for this film was around 14.6 $\mu g/cm^2$. ZnO can be etched away in acidic media as can be seen in previous reports.[54] Therefore, the absolute value of the slope in this case is higher than that of Al_2O_3, corresponding to an etch rate of 0.01259 $\mu g/cm^2/s$. Given that the density[51] of ALD ZnO is 5.61 g/cm^3, the above etch rate corresponds to 0.02 nm/s. Compared to Al_2O_3, ZnO etches 41× more rapidly than Al_2O_3.

Prior to studying the release rate of 5-ASA in acidic HCl media, the UV–vis spectrum of 5-ASA was studied. An aliquot of 5-ASA corresponding to 70 $\mu g/mL$ was pipetted into a 1 cm path length quartz cuvette. The spectrum collected is shown in Figure 6, where a peak maximum is reached at 298 nm as reported by others.[33,55] This characteristic peak is a good indicator that 5-ASA remains chemically viable through ALD coating and therefore is chosen to subsequently study the release rate of 5-ASA powder in pH 4 solution and with various coatings of ALD films.

To study the release rates of 5-ASA (uncoated and coated), powders were immersed in a pH 4 HCl solution containing a fiber optic probe connected to a UV–vis system. The probe tip was consistently placed at the same position in the beaker to negate any artifact in the measurements which might arise from variabilities in the time taken for the molecule to reach

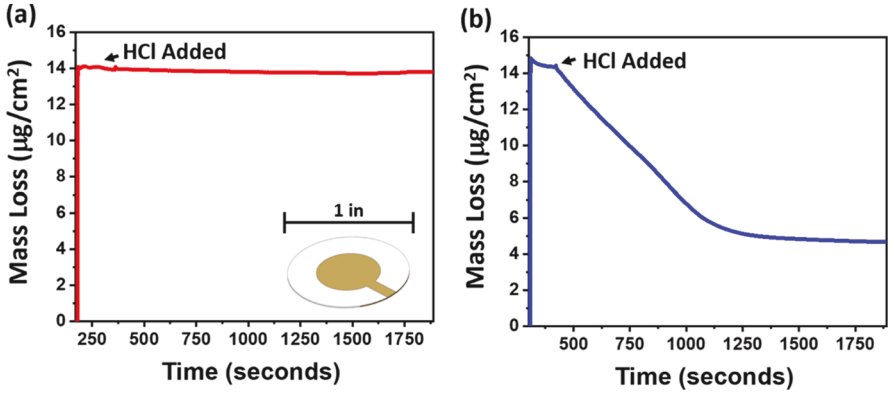

Figure 5. (a) QCM plot showing mass loss in $\mu g/cm^2$of 30 nm of Al_2O_3 in a pH 4 HCl solution. The inset on bottom right shows a typical QCM crystal with a well-defined Au electrode, further coated with ALD. (b) QCM plot showing mass loss in $\mu g/cm^2$ of 27 nm of ZnO in the pH 4 HCl solution.

https://doi.org/10.1021/acsabm.2c00750
ACS Appl. Bio Mater. XXXX, XXX, XXX–XXX

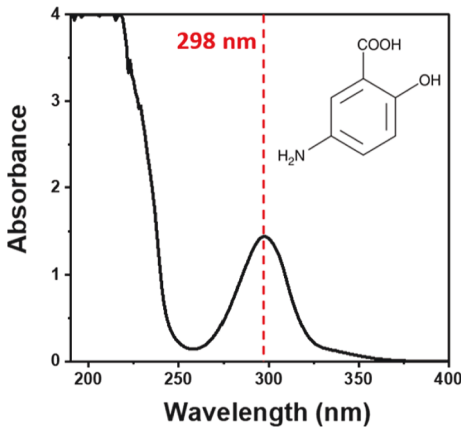

Figure 6. Representative UV−vis spectrum of 70 μg/mL concentration of 5-ASA in HCl solution.

the sensor tip. The release of 5-ASA in the solution was determined by tracking the evolution of 298 nm feature in the UV−vis spectrum over time. An example of the raw kinetic data collected is shown in Supporting Information S4.

Next, two specific studies were conducted. In the first study, the release rate of 5-ASA powders, with and without 300 cycle Al_2O_3 ALD, was studied by gathering the absorbance at 298 nm as a function of time. The powders were stirred at different rpm values using a magnetic stir bar in a pH 4 HCl solution. The justification for studying release rate as a function of stirring was to recognize that the stirring action produces mechanical attrition of the 5-ASA particles and may thus mimic gut peristalsis. The powders were exposed to three different conditions: fast stirring at 400 rpm, slow stirring at 23 rpm, and no stirring (i.e., 0 rpm). The results for all the three experiments are shown in Figure 7a−c, respectively. The gray data points correspond to the mean of three batches (triplicates) of 8 mg each of control (i.e., uncoated 5-ASA) with standard deviations provided as a filled "band" behind the data. The red data points correspond to three batches of 8 mg each of 300CyAl_2O_3@5-ASA. All time scans represent the absorption intensity of 5-ASA at 298 nm wavelength. We note that in Figure 7c the standard deviation obtained for the no stir, uncoated sample was large as there was variation in the dispersity of the uncoated 5-ASA powder from batch to batch, where some particles sank to the bottom of the solution and the rest stayed afloat. The large standard deviation does not influence the conclusions obtained between uncoated and coated batches.

Across all stirring test conditions, the 300CyAl_2O_3@5-ASA powders showed a subdued release compared to the control, uncoated powder. These results are in line with the QCM data (see Figure 5), which shows enhanced chemical stability of Al_2O_3 in the pH 4 solution. Thus, the release of 5-ASA in 300CyAl_2O_3@5-ASA can be attributed to particle attrition which leads to exposure of new, unprotected 5-ASA surfaces. The exposure of new 5-ASA surfaces lead to ready dissolution of the particles in pH 4 solution. This conclusion is further supported by the fact that the release rates for the coated samples are rpm dependent. At 400 rpm, nearly all 5-ASA-coated powder is released in 5000 s due to the high rate of mechanical attrition. On the other hand, at 23 rpm while 5-ASA is released, the absorption value at the end of 5000 s is lower than that of the control powder. This indicates that the slow rpm is unable to break down all particles, and these remain protected by the 300 cycle Al_2O_3 ALD shell. Finally, for the no stir (i.e., 0 rpm) sample, virtually no signal for 5-ASA is obtained, indicating that the particles remain intact in solution, protected by the 300 cycle Al_2O_3 ALD shell over a sustained period of time. Thus, the results from the stirring experiment reiterate the fact that particle attrition effects in the gut due to peristalsis need to be taken into account when designing nanocoatings for API powders.

In order to quantify release rate data, the following equation was adopted to model the curves

$$\mathrm{abs}(t) = \frac{P_1 t}{P_2 + t} \tag{1}$$

Here, abs(t) represents the time (t) variation of the absorbance from the UV−vis data. P_1 represents the asymptotic value in absorbance which corresponds to the full dissolution of 5-ASA in HCl. P_2 is the time taken in seconds for reaching half the absorbance saturation (i.e., the time at which absorbance is 0.5 × P_1). In Figure 7a−c, the model curves are also overlaid over the raw data points as a solid line.

A first-order kinetics equation is regularly used to describe the release rates.[56] In our case, we find the use of eq 1 justified for the following reasons. First, our first-order kinetics modeling did not yield a high goodness of fit with the data, possibly attributed to a multimechanism for release which involves (i) mechanical action involving particle breakage exposing fresh surfaces and (ii) slow shell dissolution in the

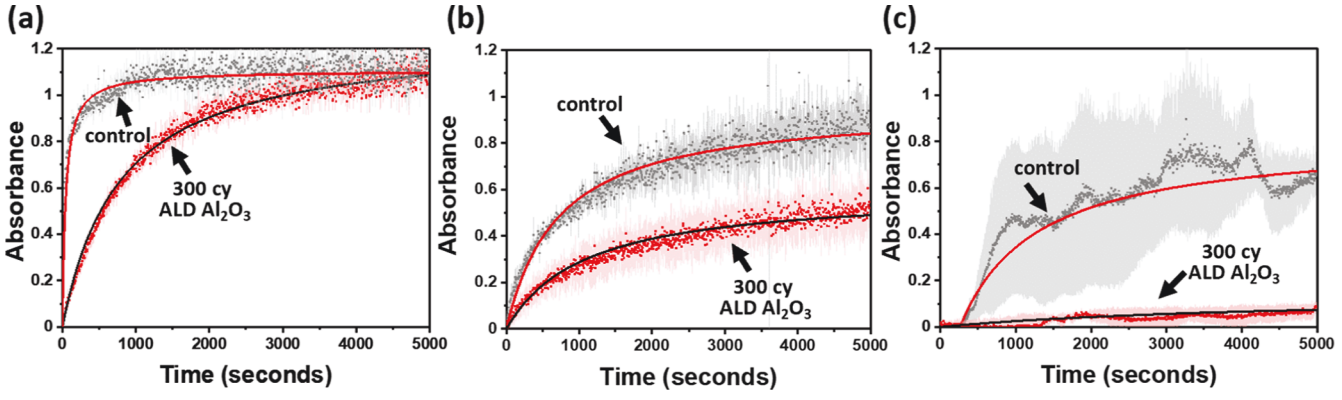

Figure 7. Release rates of control 5-ASA and 300CyAl_2O_3@5-ASA at (a) 400, (b) 23, and (c) 0 rpm. Data is obtained by averaging a set of three runs per sample, and the error associated is shown as a filled area in the background. Solid lines show fit based on eq 1 in the text.

https://doi.org/10.1021/acsabm.2c00750
ACS Appl. Bio Mater. XXXX, XXX, XXX−XXX

Table 1. Parameters P_1 and P_2 Extracted for the Release Rate Data from Figure 7a–c[a]

	P_1 (absorbance, a.u.)			P_2 (time, seconds)		
coating	400 rpm	23 rpm	no rpm	400 rpm	23 rpm	no rpm
control	1.084 ± 0.002	0.961 ± 0.005	0.818 ± 0.007	41 ± 1	712 ± 8	1023 ± 31
Al_2O_3	1.258 ± 0.003	0.595 ± 0.004	0.140 ± 0.008	784 ± 8	1070 ± 16	2686 ± 261

[a]P_1 is given in terms of absorbance (a.u.) and P_2 is provided in terms of seconds. The definitions for P_1 and P_2 are provided in the text.

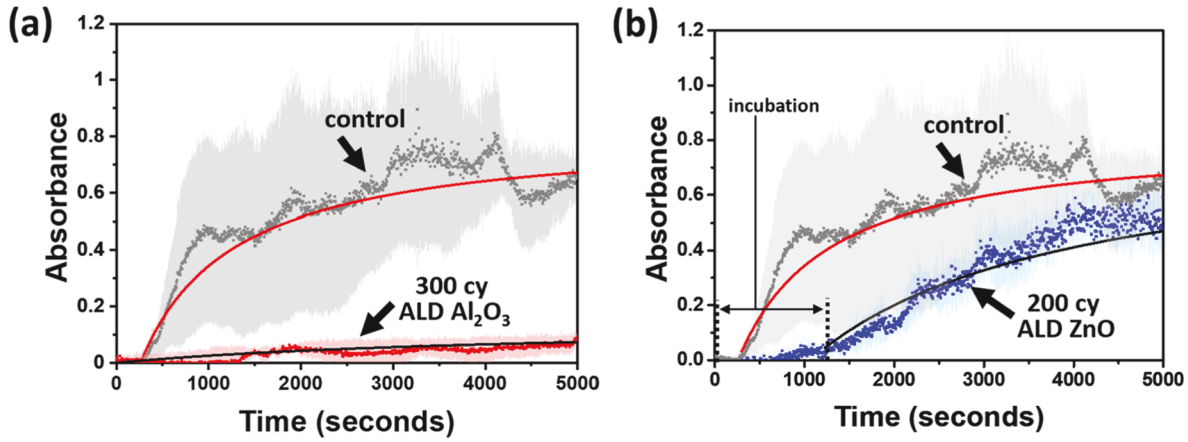

Figure 8. (a) Release rate studies under no stirring conditions of (a) control 5-ASA and 300CyAl$_2$O$_3$@5-ASA and (b) control and 200CyZnO@5-ASA. Solid lines show fits based on eq 1.

low pH solution. Second, eq 1 provides a high goodness of fit ($r^2 > 0.90$, except for control sample in the no stir case) for all the release rate data evaluated. Third, the parameters (P_1 and P_2) extracted are physically relevant. P_1 corresponds to the saturation absorbance for a specific mass loading of the 5-ASA powder. P_2 is related to the kinetics of the dissolution process which directly corresponds to the release rate of the powder. Importantly, these parameters allow quantification of the ALD coating performance on 5-ASA, which is key to comparing samples across various testing conditions and coating chemistries.

The parameters extracted from fitting eq 1 to the release rate data (average and standard deviation obtained from triplicate runs) for all powders are provided in Table 1. P_1 is found to be a function of both rpm and coating. P_1 increases with rpm and, in general, is higher for the control, uncoated powder compared to 300CyAl$_2$O$_3$@5-ASA. At 23 rpm, P_1 is 0.961 ± 0.005 for the uncoated powder and 0.595 ± 0.004 for 300CyAl$_2$O$_3$@5-ASA. Similarly, for the no stir sample, P_1 is 0.818 ± 0.007 for the uncoated powder and 0.140 ± 0.008 for 300CyAl$_2$O$_3$@5-ASA. An exception to this is found for the 400 rpm sample where P_1 for the 300CyAl$_2$O$_3$@5-ASA powder appears higher (1.258 ± 0.003) than the uncoated powder (1.084 ± 0.002). This anomaly could be attributed to the difference in dispersity of the two powders, accentuated at high rpm.

The kinetic parameter P_2 quantifies the rate of dissolution of 5-ASA in the pH 4 solution. As expected, P_2 increases with a decreasing stirring rate and is consistently higher for the coated powder than for the uncoated powder, indicating the effectiveness of the 300 cycle Al_2O_3 ALD in slowing dissolution across all stirring conditions. For example, at 400 rpm, the uncoated powder has a P_2 of 41 ± 1 s, whereas 300CyAl$_2$O$_3$@5-ASA has a P_2 of 784 ± 8 s. At 23 rpm, the uncoated powder has a P_2 of 712 ± 8 s, whereas 300CyAl$_2$O$_3$@5-ASA has a P_2 of 1070 ± 16 s. Finally, for the no stir sample, the uncoated powder has a P_2 of 1023 ± 31 s, whereas 300CyAl$_2$O$_3$@5-ASA has a P_2 of 2686 ± 261 s.

Last, the effect of two different film chemistries, 300 cycle Al_2O_3 ALD and 200 cycle ZnO ALD, was studied on the release rate of 5-ASA in the pH 4 solution. The release rate studies were conducted under no stir conditions to negate any influence of mechanical attrition of the particles. The results are shown in Figure 8a for 300CyAl$_2$O$_3$@5-ASA (same as in Figure 7c) and in Figure 8b for 200CyZnO@5-ASA.

As reported previously, 300CyAl$_2$O$_3$@5-ASA does not show significant release of 5-ASA as Al_2O_3 is stable in pH 4. However, for 200CyZnO@5-ASA, an incubation period of 1225 s is observed. Beyond this time, 5-ASA can be reliably detected in the solution. The incubation time is the time it takes for HCl to etch through the ZnO coating. From QCM studies presented earlier, the etching rate for ZnO at pH 4 is 0.02 nm/s. Therefore in 1225 s, it is expected that 24.5 nm of ZnO film will be removed. This value can be compared to the 24.7 nm final thickness of ZnO observed on 5-ASA shown in the TEM image in Figure 4a. Additionally, we see no obvious effect of the infiltrated ZnO crystals on the release rates. It is also possible that during deposition, some of the 5-ASA particles get deposited with thickness lesser than the target thickness (e.g., new particles which form during the tumbling process in the rotatory ALD reactor). The incubation period observed for 200CyZnO@5-ASA is an indication that chemical interaction between the solution and the ZnO coating (i.e., its composition and thickness) can be used to drive dissolution based on (1) the specificity of the environment (i.e., pH) and (2) time.

The fit parameters P_1 and P_2 are presented as a comparison in Table 2. The P_1 parameter for the control and 200CyZnO@5-ASA is nearly the same indicating that, eventually with the ZnO fully dissolved, the 5-ASA powder reaches its saturation absorption value of ~0.82, as in the case of control. In the same time interval, 300CyAl$_2$O$_3$@5-ASA releases 5-ASA with

https://doi.org/10.1021/acsabm.2c00750
ACS Appl. Bio Mater. XXXX, XXX, XXX−XXX

Table 2. Parameters P_1 and P_2 Extracted for the Release Rate Data from Figure 8 a,b

	P_1 (absorbance, a.u.)	P_2 (time, seconds)
coating	no rpm	no rpm
control	0.818 ± 0.007	1023 ± 31
Al_2O_3	0.140 ± 0.008	2686 ± 261
ZnO	0.820 ± 0.023	2651 ± 135

an absorbance value of 0.140. This value is 17.5% of the total absorbance recorded from the control sample. Thus, the P_1 parameter helps quantify the degree of protection that Al_2O_3 provides in a pH 4 environment.

The kinetic parameter P_2, on the other hand, is similar for 300CyAl_2O_3@5-ASA and 200CyZnO@5-ASA (2686 s vs 2651 s, respectively). Since in both cases the powder sinks to the bottom of the beaker (note: for the control, uncoated sample, the powder is dispersed at the bottom and top and hence results in lower P_2), the times involved in reaching saturation are diffusion-limited and unrelated to the powder coating quality.

CONCLUSIONS

Conformal nanoscale coatings of 38.0 nm of Al_2O_3 and 24.7 nm of ZnO on 5-ASA powders have been demonstrated using ALD. ATR-FTIR measurements and TGA on the coated powders indicate that the low temperature of ALD (120 °C) maintains the viability of the molecule. SEM reveals a needle-like morphology of 5-ASA that remains intact through the deposition process. EDS provides confirmation of the presence of Al_2O_3 and ZnO. S/TEM and associated STEM/EDS mapping of the powders indicate that ALD is uniform, pin-hole free, and conformal around the 5-ASA particles. Furthermore, the interface between Al_2O_3 and 5-ASA is found to be stable and sharp, whereas ZnO appears to limitedly diffuse inside the 5-ASA particle.

To study 5-ASA release rates in an acidic environment, the etching rates of Al_2O_3 and ZnO at pH 4 were studied using a QCM. It was found that the etching rate of ZnO is 41× more than Al_2O_3. Based on this finding, 5-ASA powder with and without ALD Al_2O_3 and ZnO layers was tested in acidic, pH 4 media. The effect of stirring, mimicking gut peristalsis, was monitored for Al_2O_3-coated 5-ASA powders. High stirring releases 5-ASA faster in the solution due to high particle attrition and exposure of new surfaces to the acidic solution. In contrast, the no stir ALD Al_2O_3-coated sample effectively slows the release of 5-ASA for at least 5000 s in the pH 4 solution. The ALD ZnO-coated 5-ASA sample under no stir conditions shows an initial "incubation period" in which 5-ASA is prevented from being released. Once ZnO is etched, 5-ASA readily dissolves in the pH 4 solution. Quantification of the release rate data indicates that the ALD Al_2O_3-coated sample releases only 17.5% of the total load in the time period it takes to release the full load of 5-ASA for the ALD ZnO-coated sample. The fundamental mechanistic studies reported here show that ALD-based nanoscale coatings can be designed to create effective barriers around 5-ASA particles. The coatings can be optimally engineered to controllably release the molecule in low-pH environments.

ASSOCIATED CONTENT

Supporting Information

The Supporting Information is available free of charge at https://pubs.acs.org/doi/10.1021/acsabm.2c00750.

FTIR data of control (uncoated) 5-ASA powder and peak assignment table, ATR-FTIR data of control 5-ASA and 200 °C heat-treated for 8 h powder, TGA of uncoated and coated 5-ASA powders with their first derivatives and, exemplary UV−vis spectra with absorbance at 298 nm of 5-ASA powder released over time (5000 s) under no stir conditions (PDF)

AUTHOR INFORMATION

Corresponding Author

Parag Banerjee − *NanoScience and Technology Center, University of Central Florida, Orlando, Florida 32826, United States; Department of Materials Science and Engineering, REACT Faculty Cluster, and Florida Solar Energy Center, University of Central Florida, Orlando, Florida 32816, United States;* orcid.org/0000-0003-0401-8155; Email: parag.banerjee@ucf.edu

Authors

Jaynlynn Sosa − *NanoScience and Technology Center, University of Central Florida, Orlando, Florida 32826, United States*

S. Novia Berriel − *Department of Materials Science and Engineering, University of Central Florida, Orlando, Florida 32816, United States*

Corbin Feit − *Department of Materials Science and Engineering, University of Central Florida, Orlando, Florida 32816, United States;* orcid.org/0000-0002-2125-5729

Taylor M. Currie − *Department of Chemistry, University of Central Florida, Orlando, Florida 32816, United States*

Lorianne R. Shultz − *Department of Chemistry, University of Central Florida, Orlando, Florida 32816, United States*

Nicholas G. Rudawski − *Research Service Centers, University of Florida, Gainesville, Florida 32611, United States*

Titel Jurca − *NanoScience and Technology Center, University of Central Florida, Orlando, Florida 32826, United States; Department of Chemistry and REACT Faculty Cluster, University of Central Florida, Orlando, Florida 32816, United States;* orcid.org/0000-0003-3656-912X

Complete contact information is available at: https://pubs.acs.org/10.1021/acsabm.2c00750

Author Contributions

The manuscript was written through contributions of all authors. All authors have given approval to the final version of the manuscript. J.S and P.B. conceptualized the experiments. J.S. conducted the experiments, provided data analysis, and wrote the manuscript. S.N.B. and C.F. helped with conducting ALD coatings on the powder. T.M.C. performed FTIR measurements and TGA. L.S. helped with training and supporting the UV−vis measurements using the in situ optical probe. N.G.R. performed TEM measurements. T.J. and P.B. contributed to the intellectual content. P.B. managed the overall project.

Funding

J.S. was partially supported by NSF award numbers 1922984 and 1908167 and AFOSR FA9550-19-1-0127. SNB was funded through SRC award number 3026.001. CF was funded

by NSF award number 1908167. The authors acknowledge funding of NSF award number 2121953. T.J. acknowledges the DOE: DE-EE0009347 for the acquisition of the FTIR microscope.

Notes

The authors declare no competing financial interest.

■ ACKNOWLEDGMENTS

The use of SEM/EDS from the Florida Solar Energy Center is kindly acknowledged.

■ REFERENCES

(1) Hajat, C.; Stein, E. The global burden of multiple chronic conditions: A narrative review. *Prev. Med. Rep.* **2018**, *12*, 284−293.
(2) Alatab, S.; Sepanlou, S. G.; Ikuta, K.; Vahedi, H.; Bisignano, C.; Safiri, S.; Sadeghi, A.; Nixon, M. R.; Abdoli, A.; Abolhassani, H.; Alipour, V.; Almadi, M. A. H.; Almasi-Hashiani, A.; Anushiravani, A.; Arabloo, J.; Atique, S.; Awasthi, A.; Badawi, A.; Baig, A. A. A.; Bhala, N.; Bijani, A.; Biondi, A.; Borzì, A. M.; Burke, K. E.; Carvalho, F.; Daryani, A.; Dubey, M.; Eftekhari, A.; Fernandes, E.; Fernandes, J. C.; Fischer, F.; Haj-Mirzaian, A.; Haj-Mirzaian, A.; Hasanzadeh, A.; Hashemian, M.; Hay, S. I.; Hoang, C. L.; Househ, M.; Ilesanmi, O. S.; Jafari Balalami, N.; James, S. L.; Kengne, A. P.; Malekzadeh, M. M.; Merat, S.; Meretoja, T. J.; Mestrovic, T.; Mirrakhimov, E. M.; Mirzaei, H.; Mohammad, K. A.; Mokdad, A. H.; Monasta, L.; Negoi, I.; Nguyen, T. H.; Nguyen, C. T.; Pourshams, A.; Poustchi, H.; Rabiee, M.; Rabiee, N.; Ramezanzadeh, K.; Rawaf, D. L.; Rawaf, S.; Rezaei, N.; Robinson, S. R.; Ronfani, L.; Saxena, S.; Sepehrimanesh, M.; Shaikh, M. A.; Sharafi, Z.; Sharif, M.; Siabani, S.; Sima, A. R.; Singh, J. A.; Soheili, A.; Sotoudehmanesh, R.; Suleria, H. A. R.; Tesfay, B. E.; Tran, B.; Tsoi, D.; Vacante, M.; Wondmieneh, A. B.; Zarghi, A.; Zhang, Z.-J.; Dirac, M.; Malekzadeh, R.; Naghavi, M. The global, regional, and national burden of inflammatory bowel disease in 195 countries and territories, 1990−2017: a systematic analysis for the Global Burden of Disease Study 2017. *Lancet Gastroenterol. Hepatol.* **2020**, *5*, 17−30.
(3) Campregher, C.; Gasche, C. Aminosalicylates. *Best Pract. Res., Clin. Gastroenterol.* **2011**, *25*, 535−546.
(4) Ahnfelt-Rønne, I.; Nielsen, O. H.; Christensen, A.; Langholz, E.; Binder, V.; Riis, P. Clinical evidence supporting the radical scavenger mechanism of 5-aminosalicylic acid. *Gastroenterology* **1990**, *98*, 1162−1169.
(5) MacDermott, R. P. Progress in understanding the mechanisms of action of 5-aminosalicylic acid. *Am. J. Gastroenterol.* **2000**, *95*, 3343.
(6) Peskar, B.; Dreyling, K.; May, B.; Schaarschmidt, K.; Goebell, H. Possible mode of action of 5-aminosalicylic acid. *Dig. Dis. Sci.* **1987**, *32*, S51−S56.
(7) Chuong, M. C.; Christensen, J. M.; Ayres, J. W. New Dissolution Method for Mesalamine Tablets and Capsules. *Dissolution Technol.* **2008**, *15*, 7−14.
(8) Qiu, Y.; Lee, P. I. *Rational Design of Oral Modified-Release Drug Delivery Systems*; Elsevier, 2017; pp 519−554.
(9) Anderson, R. J.; Kirk, L. M. Methods of improving patient compliance in chronic disease states. *Arch. Intern. Med.* **1982**, *142*, 1673−1675.
(10) Eraker, S. A.; Kirscht, J. P.; Becker, M. H. Understanding and improving patient compliance. *Ann. Intern. Med.* **1984**, *100*, 258−268.
(11) Dunbar-Jacob, J.; Mortimer-Stephens, M. Treatment adherence in chronic disease. *J. Clin. Epidemiol.* **2001**, *54*, S57−S60.
(12) Shale, M.; Riley, S. Studies of compliance with delayed-release mesalazine therapy in patients with inflammatory bowel disease. *Aliment. Pharmacol. Ther.* **2003**, *18*, 191−198.
(13) Thakral, S.; Thakral, N. K.; Majumdar, D. K. Eudragit: a technology evaluation. *Expert Opin. Drug Discovery* **2013**, *10*, 131−149.
(14) George, S. M. Atomic layer deposition: an overview. *Chem. Rev.* **2010**, *110*, 111−131.
(15) Johnson, R. W.; Hultqvist, A.; Bent, S. F. A brief review of atomic layer deposition: from fundamentals to applications. *Mater. Today* **2014**, *17*, 236−246.
(16) Leskelä, M.; Ritala, M. Atomic layer deposition (ALD): From precursors to thin film structures. *Thin Solid Films* **2002**, *409*, 138−146.
(17) Puurunen, R. L. Surface chemistry of atomic layer deposition: A case study for the trimethylaluminum/water process. *J. Appl. Phys.* **2005**, *97*, 121301.
(18) Miikkulainen, V.; Leskelä, M.; Ritala, M.; Puurunen, R. L. Crystallinity of inorganic films grown by atomic layer deposition: Overview and general trends. *J. Appl. Phys.* **2013**, *113*, 021301.
(19) Dillon, A. C.; Ott, A. W.; Way, J. D.; George, S. M. Surface-Chemistry of Al_2O_3 Deposition Using $Al(CH_3)_3$ and H_2O in a Binary Reaction Sequence. *Surf. Sci.* **1995**, *322*, 230−242.
(20) Yousfi, E. B.; Fouache, J.; Lincot, D. Study of atomic layer epitaxy of zinc oxide by in-situ quartz crystal microgravimetry. *Appl. Surf. Sci.* **2000**, *153*, 223−234.
(21) Sammelselg, V.; Rosental, A.; Tarre, A.; Niinisto, L.; Heiskanen, K.; Ilmonen, K.; Johansson, L.-S.; Uustare, T. TiO_2 thin films by atomic layer deposition: A case of uneven growth at low temperature. *Appl. Surf. Sci.* **1998**, *134*, 78−86.
(22) Dias, V.; Maciel, H.; Fraga, M.; Lobo, A. O.; Pessoa, R.; Marciano, F. R. Atomic Layer Deposited TiO_2 and Al_2O_3 Thin Films as Coatings for Aluminum Food Packaging Application. *Materials* **2019**, *12*, 682.
(23) Petrochenko, P. E.; Kumar, G.; Fu, W.; Zhang, Q.; Zheng, J.; Liang, C.; Goering, P. L.; Narayan, R. J. Nanoporous Aluminum Oxide Membranes Coated with Atomic Layer Deposition-Grown Titanium Dioxide for Biomedical Applications: An In Vitro Evaluation. *J. Biomed. Nanotechnol.* **2015**, *11*, 2275−2285.
(24) Osorio, D.; Lopez, J.; Tiznado, H.; Farias, M. H.; Hernandez-Landaverde, M. A.; Ramirez-Cardona, M.; Yañez-Limon, J. M.; Gutierrez, J. O.; Caicedo, J. C.; Zambrano, G. Structure and Surface Morphology Effect on the Cytotoxicity of $[Al_2O_3/ZnO]$ Nano-laminates on/316L SS Growth by Atomic Layer Deposition (ALD). *Crystals* **2020**, *10*, 620.
(25) Chazot, M.; Kostogiannes, A.; Julian, M.; Feit, C.; Sosa, J.; Kang, M.; Blanco, C.; Cook, J.; Rodriguez, V.; Adamietz, F.; Verreault, D.; Banerjee, P.; Schepler, K.; Richardson, M. C.; Richardson, K. A. Enhancement of ZnSe stability during optical composite processing via atomic layer deposition. *J. Non-Cryst. Solids* **2022**, *576*, 121259.
(26) Hirschberg, C.; Jensen, N. S.; Boetker, J.; Madsen, A. Ø.; Kääriäinen, T. O.; Kääriäinen, M.-L.; Hoppu, P.; George, S. M.; Murtomaa, M.; Sun, C. C.; Risbo, J.; Rantanen, J. Improving Powder Characteristics by Surface Modification Using Atomic Layer Deposition. *Org. Process Res. Dev.* **2019**, *23*, 2362−2368.
(27) Kääriäinen, T. O.; Kemell, M.; Vehkamäki, M.; Kääriäinen, M.-L.; Correia, A.; Santos, H. A.; Bimbo, L. M.; Hirvonen, J.; Hoppu, P.; George, S. M.; Cameron, D. C.; Ritala, M.; Leskelä, M. Surface modification of acetaminophen particles by atomic layer deposition. *Int. J. Pharm.* **2017**, *525*, 160−174.
(28) Hellrup, J.; Rooth, M.; Mårtensson, E.; Sigfridsson, K.; Johansson, A. Nanoshells prepared by atomic layer deposition−long acting depots of indomethacin. *Eur. J. Pharm. Biopharm.* **2019**, *140*, 60−66.
(29) Zhang, D.; Quayle, M. J.; Petersson, G.; van Ommen, J. R.; Folestad, S. Atomic scale surface engineering of micro- to nano-sized pharmaceutical particles for drug delivery applications. *Nanoscale* **2017**, *9*, 11410−11417.
(30) La Zara, D.; Sun, F.; Zhang, F.; Franek, F.; Balogh Sivars, K.; Horndahl, J.; Bates, S.; Brännström, M.; Ewing, P.; Quayle, M. J.; Petersson, G.; Folestad, S.; van Ommen, J. R. Controlled Pulmonary Delivery of Carrier-Free Budesonide Dry Powder by Atomic Layer Deposition. *ACS Nano* **2021**, *15*, 6684−6698.
(31) Garcea, R. L.; Meinerz, N. M.; Dong, M.; Funke, H.; Ghazvini, S.; Randolph, T. W. Single-administration, thermostable human papillomavirus vaccines prepared with atomic layer deposition technology. *npj Vaccines* **2020**, *5*, 45.

https://doi.org/10.1021/acsabm.2c00750
ACS Appl. Bio Mater. XXXX, XXX, XXX−XXX

(32) Adhikari, S.; Selvaraj, S.; Kim, D.-H. Progress in Powder Coating Technology Using Atomic Layer Deposition. *Adv. Mater. Interfaces* **2018**, *5*, 1800581.
(33) Acharjya, S. K.; Sahu, A.; Das, S.; Sagar, P.; Annapurna, M. M. Spectrophotometric methods for the determination of mesalamine in bulk and pharmaceutical dosage forms. *Indian J. Pharm. Educ. Res.* **2010**, *1*, 348.
(34) Movahedinia, H.; Shahidi-Zandi, M.; Kazemipour, M. Investigation of 5-aminosalicylic acid (Mesalazine Drug) as a Corrosion Inhibitor for Carbon Steel in Sulfuric Acid Solution. *Int. J. Electrochem. Sci.* **2021**, *16*, 210228.
(35) Hu, D.; Liu, L.; Chen, W.; Li, S.; Zhao, Y. A novel preparation method for 5-aminosalicylic acid loaded Eudragit S100 nanoparticles. *Int. J. Mol. Sci.* **2012**, *13*, 6454−6468.
(36) Dumitru, M. V.; Sandu, T.; Ciurlică, A. L.; Neblea, I. E.; Trică, B.; Ghebaur, A.; Gârea, S. A.; Iovu, H.; Sârbu, A.; Iordache, T. V. Organically modified montmorillonite as pH versatile carriers for delivery of 5-aminosalicylic acid. *Appl. Clay Sci.* **2022**, *218*, 106415.
(37) Duan, H.; Lü, S.; Gao, C.; Bai, X.; Qin, H.; Wei, Y.; Wu, X.; Liu, M. Mucoadhesive microparticulates based on polysaccharide for target dual drug delivery of 5-aminosalicylic acid and curcumin to inflamed colon. *Colloids Surf., B* **2016**, *145*, 510−519.
(38) Myers, T. J.; Cano, A. M.; Lancaster, D. K.; Clancey, J. W.; George, S. M. Conversion reactions in atomic layer processing with emphasis on ZnO conversion to Al_2O_3 by trimethylaluminum. *J. Vac. Sci. Technol., A* **2021**, *39*, 021001.
(39) Lu, S.; Wang, H.; Zhou, J.; Wu, X.; Qin, W. Atomic layer deposition of ZnO on carbon black as nanostructured anode materials for high-performance lithium-ion batteries. *Nanoscale* **2017**, *9*, 1184−1192.
(40) Boyadjiev, S. I.; Georgieva, V.; Yordanov, R.; Raicheva, Z.; Szilágyi, I. M. Preparation and characterization of ALD deposited ZnO thin films studied for gas sensors. *Appl. Surf. Sci.* **2016**, *387*, 1230−1235.
(41) Schmitt, H.; Creton, N.; Prashantha, K.; Soulestin, J.; Lacrampe, M. F.; Krawczak, P. Melt-blended halloysite nanotubes/wheat starch nanocomposites as drug delivery system. *Polym. Eng. Sci.* **2015**, *55*, 573−580.
(42) Pawar, A. R.; Mundhe, P. V.; Deshmukh, V. K.; Pandhare, R. B.; Nandgude, T. D. Enrichment of aqueous solubility and dissolution profile of mesalamine: In vitro evaluation of solid dispersion. *J. Pharm. Biol. Sci.* **2021**, *9*, 127−135.
(43) Narayan Sahoo, R.; De, A.; Kataria, V.; Mallick, S. Solvent-free Hot Melt Extrusion Technique in Improving Mesalamine Release for Better Management of Inflammatory Bowel Disease. *Indian J. Pharm. Educ. Res.* **2019**, *53*, s554−s562.
(44) *Energy Table for EDS Analysis* (Document ID: JEC6101C602A). www.jeol.com.
(45) George, S.; Ott, A.; Klaus, J. Surface chemistry for atomic layer growth. *J. Phys. Chem.* **1996**, *100*, 13121−13131.
(46) Wu, F.; Banerjee, S.; Li, H.; Myung, Y.; Banerjee, P. Indirect Phase Transformation of CuO to Cu_2O on a Nanowire Surface. *Langmuir* **2016**, *32*, 4485−4493.
(47) Perez, I.; Robertson, E.; Banerjee, P.; Henn-Lecordier, L.; Son, S. J.; Lee, S. B.; Rubloff, G. W. TEM-based metrology for HfO_2 layers and nanotubes formed in anodic aluminum oxide nanopore structures. *Small* **2008**, *4*, 1223−1232.
(48) Gao, Z.; Wu, F.; Myung, Y.; Fei, R.; Kanjolia, R.; Yang, L.; Banerjee, P. Standing and Sitting Adlayers in Atomic Layer Deposition of ZnO. *J. Vac. Sci. Technol., A* **2016**, *34*, 01A143.
(49) Guziewicz, E.; Kowalik, I. A.; Godlewski, M.; Kopalko, K.; Osinniy, V.; Wójcik, A.; Yatsunenko, S.; Łusakowska, E.; Paszkowicz, W.; Guziewicz, M. Extremely low temperature growth of ZnO by atomic layer deposition. *J. Appl. Phys.* **2008**, *103*, 033515.
(50) Bacsa, J.; Hanke, F.; Hindley, S.; Odedra, R.; Darling, G. R.; Jones, A. C.; Steiner, A. The Solid-State Structures of Dimethylzinc and Diethylzinc. *Angew. Chem., Int. Ed.* **2011**, *50*, 11685−11687.
(51) Jensen, J. M.; Oelkers, A. B.; Toivola, R.; Johnson, D. C.; Elam, J. W.; George, S. M. X-ray reflectivity characterization of ZnO/Al_2O_3 multilayers prepared by atomic layer deposition. *Chem. Mater.* **2002**, *14*, 2276−2282.
(52) Willis, S. A.; McGuinness, E. K.; Li, Y.; Losego, M. D. Re-examination of the Aqueous Stability of Atomic Layer Deposited (ALD) Amorphous Alumina (Al2O3) Thin Films and the Use of a Postdeposition Air Plasma Anneal to Enhance Stability. *Langmuir* **2021**, *37*, 14509−14519.
(53) Correa, G. C.; Bao, B.; Strandwitz, N. C. Chemical Stability of Titania and Alumina Thin Films Formed by Atomic Layer Deposition. *ACS Appl. Mater. Interfaces* **2015**, *7*, 14816−14821.
(54) Sun, K. G.; Li, Y. V.; Saint John, D. B.; Jackson, T. N. pH-Controlled Selective Etching of Al_2O_3 over ZnO. *ACS Appl. Mater. Interfaces* **2014**, *6*, 7028−7031.
(55) Kaur, H.; Kumar, S.; Kukkar, D.; Kaur, I.; Singh, K.; Bharadwaj, L. M. Transportation of drug-(polystyrene bead) conjugate by actomyosin motor system. *J. Biomed. Nanotechnol.* **2010**, *6*, 279−286.
(56) Suhail, M.; Shao, Y. F.; Vu, Q. L.; Wu, P. C. Designing of pH-Sensitive Hydrogels for Colon Targeted Drug Delivery; Characterization and In Vitro Evaluation. *Gels* **2022**, *8*, 155.

https://doi.org/10.1021/acsabm.2c00750
ACS Appl. Bio Mater. XXXX, XXX, XXX−XXX